Angular distributions of protons scattered by Ar40 nuclei with excitation of the 2+(1.46 MeV) and 3−(3.68 MeV) collective levels for incident energies of 25.1, 32.5, and 40.7 MeV

7 authors, including:

Nazmi Turan Okumuşoğlu
Ondokuz Mayıs Üniversitesi
29 PUBLICATIONS **589** CITATIONS

SEE PROFILE

Filiz Korkmaz Görür
Bolu Abant Izzet Baysal University
18 PUBLICATIONS **845** CITATIONS

SEE PROFILE

J. Birchall
University of Manitoba
155 PUBLICATIONS **1,608** CITATIONS

SEE PROFILE

Efrem Sh. Soukhovitski
Joint Institute for Power and Nuclear Research - SOSNY
78 PUBLICATIONS **3,628** CITATIONS

SEE PROFILE

Angular distributions of protons scattered by ^{40}Ar nuclei with excitation of the 2^+(1.46 MeV) and 3^-(3.68 MeV) collective levels for incident energies of 25.1, 32.5, and 40.7 MeV

N. T. Okumuşoğlu[*] and F. Korkmaz Gorur
Department of Physics, Faculty of Art and Science, Rize University, Rize, 53100, Turkey

J. Birchall
Department of Physics & Astronomy, University of Manitoba, Winnipeg, Manitoba, Canada R3T 2N2

E. Sh. Soukhovitskii
Joint Institute for Energy and Nuclear Research, 220109, Minsk-Sosny, Belarus

R. Capote
Nuclear Data Section, International Atomic Energy Agency, Wagramerstrasse 5, Vienna A-1400, Austria

J. M. Quesada
Departamento de Física Atómica, Molecular y Nuclear, Universidad de Sevilla, Ap.1065, E-41080 Sevilla, Spain

S. Chiba[†]
Advanced Science Research Center, Japan Atomic Energy Agency, Tokai, Naka, Ibaraki 319-1195, Japan

Elastic and inelastic scattering of unpolarized and polarized protons by ^{40}Ar nuclei for incident energies between 20 and 50 MeV has been studied by reanalyzing experimental scattering spectra for the 2^+(1.46 MeV) and 3^-(3.68 MeV) levels in the angular range 30°–160° for incident protons of energies of 25.1, 32.5, and 40.7 MeV. An isospin dependent soft-rotator coupled-channels optical model with the potential containing a dispersive term with a nonlocal contribution is used to analyze the data.

I. INTRODUCTION

In the nucleon-nucleus interaction at low- to medium-energy regions, the excitation of low-lying collective levels, is one of the dominant reaction processes, determining the high-energy portion of the inelastic spectra. It is therefore essentially important to understand systematically underlying reaction mechanisms that reflect the properties of these excited states. Furthermore, it is also important from application points of view because nucleon-induced reactions are utilized in many applied fields such as nuclear energy (including transmutation of nuclear wastes), radiation therapy, radiation-dose analysis of aircraft pilots, and/or electronic devices due to air-shower, and so on.

We have successfully applied a coupled-channels method based on soft-rotator model (SRM-CC) for a number of nuclei to describe simultaneously the collective level structure excitation of them in nucleon-induced reactions and electromagnetic transitions among them. Basically, the model, due to the underlying physics, is expected to be applicable to rotational nuclei. Nevertheless, we have seen so far that it can be quite successfully applied also to so-called "vibrational" nuclei as an "effective" model [1,2].

However, applicability of SRM-CC in a mass region below $A = 50$ is still an open question although we have seen a good success of it for ^{12}C [3] and ^{28,30}Si [4]. In this mass range, the number of single-particle orbits is rather small and separation of them is quite large. This indicates that shell effects, e.g., how nucleons are distributed among various single-particle orbits and how they couple to determine the total spin, have a large influence on the nature of the excited states. Under these circumstances, it is not obvious at all if the SRM is effective for these light nuclei, because the collective model, on which SRM is based, is valid only when contributions of many shells are accounted and averaged.

In case of ^{40}Ar, it has a small quadrupole moment and a large $B(E2)$ value. This fact indicates that it is more like a vibrational than a rotational nucleus. However, degeneracy of the 0_2^+, 2_2^+, and 4_1^+ levels are broken to a significant extent, implying that it is not a simple harmonic-vibrational type nucleus. In this work, we tackle to describe the collective levels and nucleon-induced reaction of ^{40}Ar in terms of SRM-CC to investigate how it works in light-mass region and to extract nuclear parameters in SRM and optical model potentials (OMP) for ^{40}Ar.

Elastic scattering of unpolarized and polarized protons by ^{40}Ar nuclei in the incident energy region 20–50 MeV has been

---

[*]Electronic address: nazmituran@superonline.com

[†]On leave from the Department of Physics, Faculty of Art and Science, 19 Mayis University, Samsun, Turkey.

a subject of a number of studies already ([5] and references therein). In most of these studies experimental results are used for the determination of the optical model potentials. Almost all of the experimental scattering data available are for elastic scattering. The only inelastic polarization results are the data of Rush *et al.* [6] for incident protons of 30.4 and 49.4 MeV measured only for the first 2_1^+ level at 1.46- MeV excitation. We have now reanalyzed our raw scattering spectra [5] which were used before by us to determine the elastic-scattering data, to make available data for the 2^+(1.46 MeV) and negative-parity level 3^-(3.68 MeV) in a wide angular range. With this it became possible to analyze the available data using a coupled-channels method. So the main aim of this work is the determination and the analysis of angular distributions of 25.1-, 32.5-, and 40.7- MeV incident protons inelastically scattered populating the 2^+(1.46 MeV) and 3^-(3.68MeV) levels of ^{40}Ar, together with the elastic data and available neutron total cross sections. Analysis of this data is achieved using the dispersive soft-rotator coupled-channels model to determine optical model potentials, allowing the prediction of nucleon optical cross sections up to at least 100 MeV.

II. MEASUREMENT OF PROTON-^{40}AR ANGULAR DISTRIBUTIONS AT INCIDENT ENERGIES OF 25.1, 32.5, AND 40.7 MEV

A. Experimental setup and method

At the time of measurements of the elastic scattering of polarized protons at 25.1, 32.5, and 40.7 MeV and the appropriate analyzing powers [5], inelastic-scattering data were also obtained for the 1.46-, 3.70-, and 4.49- MeV states of ^{40}Ar with reasonable statistics. Protons with a polarization of approximately 82% were accelerated to the desired energies by the 88-inch cyclotron of Lawrence Berkeley Laboratory. The target consisted of argon gas contained in a cell at 2 atm. Four sets of detector telescopes were used. The telescopes were located symmetrically with respect to the incoming beam so that measurements of analyzing power could be made at two angles simultaneously. Each of the telescopes comprised a 0.5-mm passing detector (ΔE) and a stopping detector (E) with a total depletion depth of 8 mm. The ΔE-E systems were used for particle identification. Collimators defined a geometry factor [7] of 3.0×10^{-6} cm.sr and provided an angular resolution of $\pm 0.5°$ (laboratory). The beam polarimeter was downstream from the argon target and consisted of a gaseous ^{4}He target maintained at a pressure of 2 atm. The protons elastically scattered by the ^{4}He target were detected by two telescopes positioned symmetrically with respect to the beam at $77.5°$ at 25.1 MeV and 32.5 MeV and at $120°$ at 40.7 MeV. The energy of the beam at the polarimeter was degraded by aluminum foils to values at which $p-^4$He analyzing power calibration points exist [8](24.0, 32.2, and 39.8 MeV respectively). The polarization of the beam was flipped automatically whenever a fixed charge was accumulated in the Faraday cup (approximately once a second) and the data were routed accordingly.
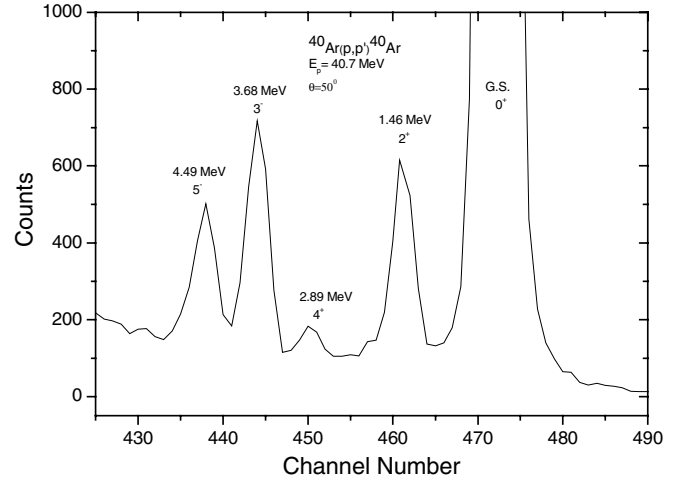

FIG. 1. Typical proton spectra.

B. Data analysis and experimental results

A typical spectrum for ^{40}Ar(p, p')^{40}Ar scattering at 25.1- MeV incoming proton energy is shown in Fig. 1. In the analysis of the data, for each incoming proton energy, E, angle θ, and excited state, the measured number of counts corrected for background, $N(\theta)$, was obtained. The differential cross section was determined by using the formula for a gas target given by:

$$\frac{d\sigma}{d\Omega} = \frac{N(\theta)\sin\theta}{R_0 nG}, \tag{1}$$

where n is the number of incoming protons, R_0 is the number of scattering centers per unit volume, and G is the geometrical factor of Silverstein for a gas target.

In the experiment also the scattering asymmetry $\varepsilon(\theta, E)$ was measured for each of the excited states considered. The asymmetry is calculated from the numbers of counts corrected for background in the left and right telescopes for beam spin up and down, namely from N_{LU}, N_{RU}, N_{LD}, and N_{RD} by using the following relations.

$$\varepsilon(\theta, E) = (r - 1)/(r + 1) \tag{2}$$

with

$$r = [(N_{LU}N_{RD})/(N_{LD}N_{RU})]^{1/2}. \tag{3}$$

The proton analyzing power $A_y(\theta, E)$ at each beam energy and laboratory angle was calculated from the corresponding asymmetry $\varepsilon(\theta, E)$ by the standard formula

$$A_y(\theta, E) = \varepsilon(\theta, E)/P, \tag{4}$$

where P is the beam polarization.

Angular distributions for cross-sections and analyzing powers of inelastically scattered protons at incident energies of 25.1, 32.5, and 40.7 MeV with the associated statistical errors are presented in Figs. 2–4, respectively. Systematic errors in analyzing powers were minimized by using symmetrical detector telescopes on either side of the beam and automatically flipping the beam polarization. Results of theoretical calculations are also shown in the figures, with the details discussed in Sec. III.
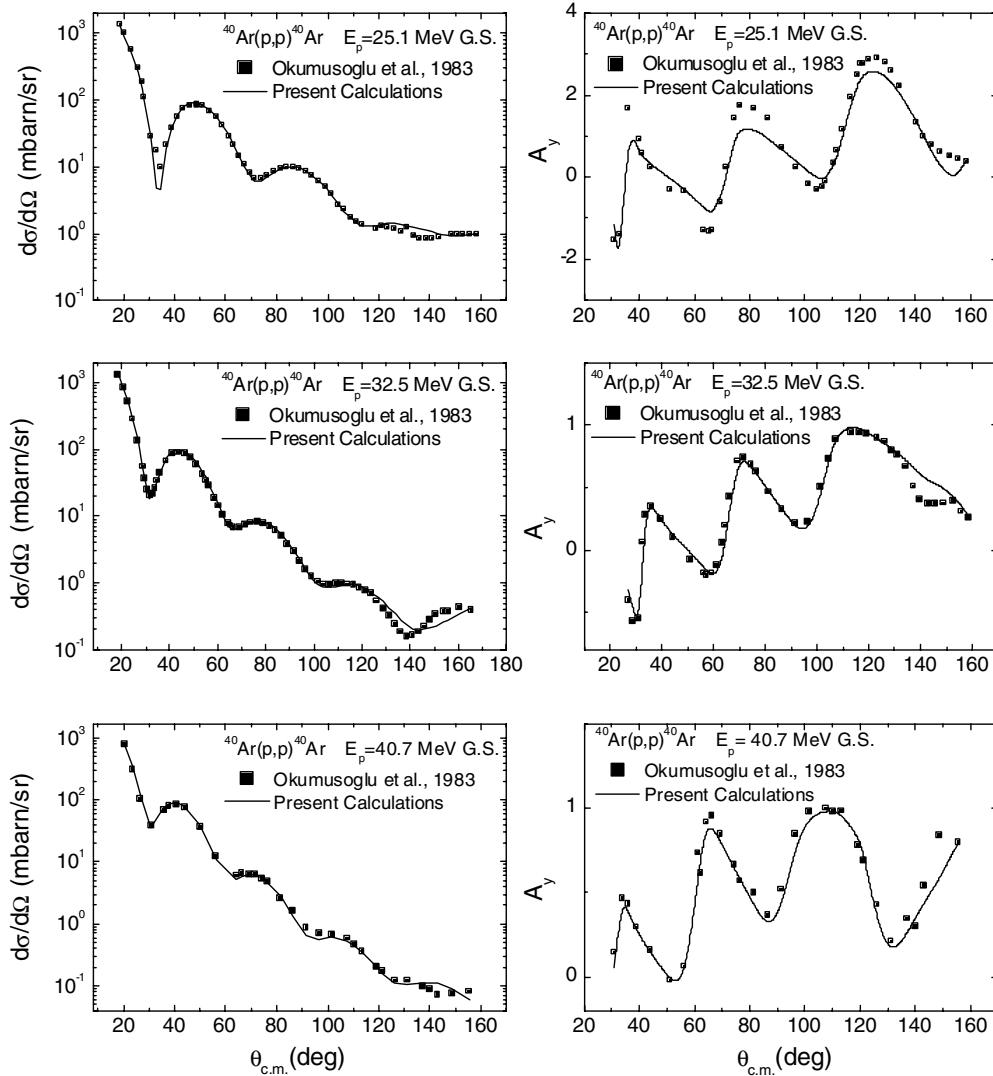
FIG. 2. Elastic angular distributions (left) and analyzing powers (right).

III. ANALYSIS USING COUPLED-CHANNELS BASED ON THE SOFT-ROTATOR MODEL WITH DISPERSIVE OPTICAL POTENTIAL FORMALISM

We used a coupled-channels optical model with coupling based on soft-rotator nuclear model (SRM) wave functions to analyze the scattering data. SRM used to build coupling for coupled-channels optical model calculations is described elsewhere [9] and is widely used for sophisticated optical data analysis and cross-section predictions for nucleons (both neutrons and protons simultaneously) interacting with nuclei at least up to 200- MeV incident energies. Not long ago this model was extended to use an optical potential with dispersion relationships between the real and imaginary parts [10]. Such extension of the model allows a significant reduction in the number of optical potential parameters to be used for the analyses, making them more physically grounded and thus the results of such analyses are more reliable. We decided to apply this optical potential model for our data analyses as it was demonstrated by analyses of actinides [10] and tungsten data [11] that such an approach is much more reliable.

As usual we assumed that the low-lying excited states observed in even-even nonspherical ^{40}Ar nuclei can be described as a combination of rotation, β-quadrupole and octupole vibrations, and γ-quadrupole vibrations. Nuclear Hamiltonian parameters determining soft-rotator nuclear wave functions were determined to describe low-lying collective levels of ^{40}Ar. We could describe with reasonable accuracy eight levels of ^{40}Ar. A comparison of experimental level energies with those predicted by the model with the Hamiltonian parameters adjusted is shown in Fig. 5. Nuclear Hamiltonian parameters producing high-quality fits to the ^{40}Ar data are given in Table I. For the meaning of the soft rotator nuclear model Hamiltonian parameters and the theory see Ref. [12].

TABLE I. Nuclear Hamiltonian parameters of ^{40}Ar.

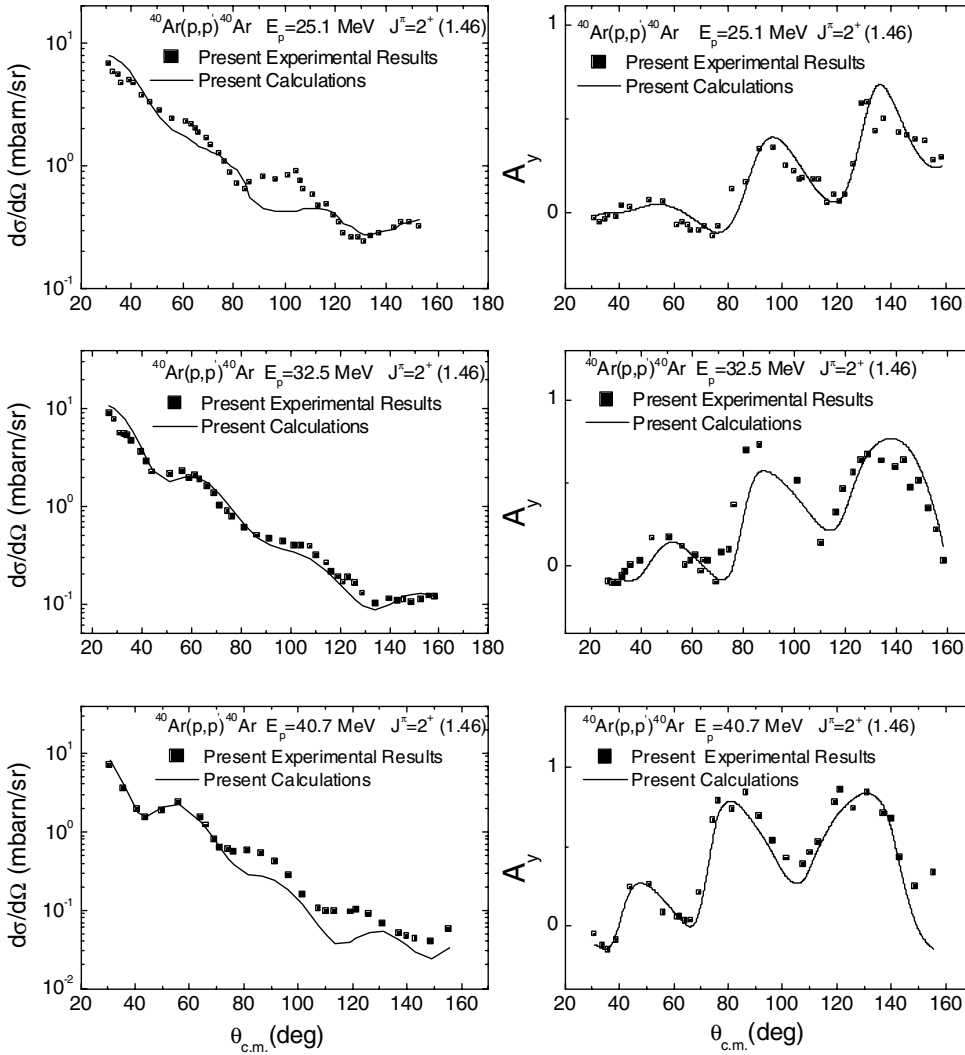|			
$\hbar w_0 = 1.1539$	$a_{42} = 0.03084$	$\gamma_4 = 0.09777$	$\gamma_0 = 0.51868$
$\mu_{\beta_{20}} = 2.0585$	$\eta = 0.00002$	$\mu_\epsilon = 0.58029$	$\delta_4 = 0.69282$
$a_{32} = 0.02658$	$\mu_{\gamma_0} = 0.1958$	$\delta_n = 4.7885$	

FIG. 3. Inelastic angular distributions (left) and analyzing powers (right) for proton scattering to the 2^+ level of ^{40}Ar.

Soft-rotator nuclear wave functions with the above parameters describing low-lying collective levels of ^{40}Ar were used to build coupling for CC optical model calculations. The coupling scheme used for the calculations is shown in Fig. 6. One can see that each of eight levels was coupled to the ground state level as well as with all the other levels coupled in these CC optical model calculations.

The optical model potential used was taken to be a standard Woods-Saxon form, but with account for the deformed nuclear shapes. The general formulation used is described in Ref. [10]. Here we give only an overview.

The optical model potential is written as

$$
\begin{aligned}
&V[r, R(\theta', \varphi'), E] \\
&= -\left[V_{\mathrm{HF}}(E) + \Delta V_{\mathrm{HF}}^{\mathrm{Coul}}(E)\right] f_{\mathrm{WS}}[r, R_{\mathrm{HF}}(\theta', \varphi')] \\
&\quad - \left[\Delta V_v(E) + \Delta V_v^{\mathrm{Coul}}(E) + i W_v(E)\right] f_{\mathrm{ws}}[r, R_v(\theta', \varphi')] \\
&\quad - \left[\Delta V_s(E) + \Delta V_s^{\mathrm{Coul}}(E) + i W_s(E)\right] g_{\mathrm{ws}}[r, R_s(\theta', \varphi')] \\
&\quad + \left(\frac{\hbar}{m_\pi c}\right)^2 [V_{\mathrm{so}}(E) + \Delta V_{\mathrm{so}}(E) + i W_{\mathrm{so}}(E)] \\
&\quad \times \frac{1}{r}\frac{d}{dr} f_{\mathrm{WS}}(r, R_{\mathrm{so}})(\hat{\sigma} \cdot \hat{L}) + V_{\mathrm{Coul}}[r, R_c(\theta', \varphi')], \quad (5)
\end{aligned}
$$

where the first term is the real smooth volume potential $V_{\mathrm{HF}}(E)$ and its corresponding Coulomb correction $\Delta V_{\mathrm{HF}}^{\mathrm{Coul}}(E) = -C_{\mathrm{Coul}}\frac{ZZ'e^2}{A^{1/3}}\frac{d}{dE}[V_{\mathrm{HF}}(E)]$. Similar Coulomb correction terms $\Delta V_v^{\mathrm{Coul}}(E)$ and $\Delta V_s^{\mathrm{Coul}}(E)$ are also calculated for volume $\Delta V_v(E)$ and surface $\Delta V_s(E)$ dispersive contributions to the real potential. Successive complex-valued terms are the volume, surface, and spin-orbit potentials, all containing the corresponding dispersive contributions $\Delta V_v(E)$, $\Delta V_s(E)$, and $\Delta V_{\mathrm{so}}(E)$. The geometrical form factors are given as

$$
\begin{aligned}
&f_{\mathrm{ws}}[r, R_i(\theta', \varphi')] = (1 + \exp\{[r - R_i(\theta', \varphi')]/a_i\})^{-1}, \\
&i = \mathrm{HF}, v \quad f_{\mathrm{ws}}(r, R_{\mathrm{so}}) = \{1 + \exp[(r - R_{\mathrm{so}})/a_{\mathrm{so}}]\}^{-1}, \\
&g_{\mathrm{ws}}[r, R_s(\theta', \varphi')] = -4a_s \frac{d}{dr} f[r, R_s(\theta', \varphi')] \quad (6)
\end{aligned}
$$

where $R_i(\theta', \varphi')$ denotes the deformed radii with the deformations considered, while spin-orbit potential is considered to be not deformed. The Coulomb potential $V_{\mathrm{Coul}}[r, R_c(\theta', \varphi')]$ was calculated using a multipole expansion of a charged ellipsoid with uniform charge density within the Coulomb radius R_c and zero outside as suggested by Satchler *et al.* [13]. The spherical term of the Coulomb potential was calculated
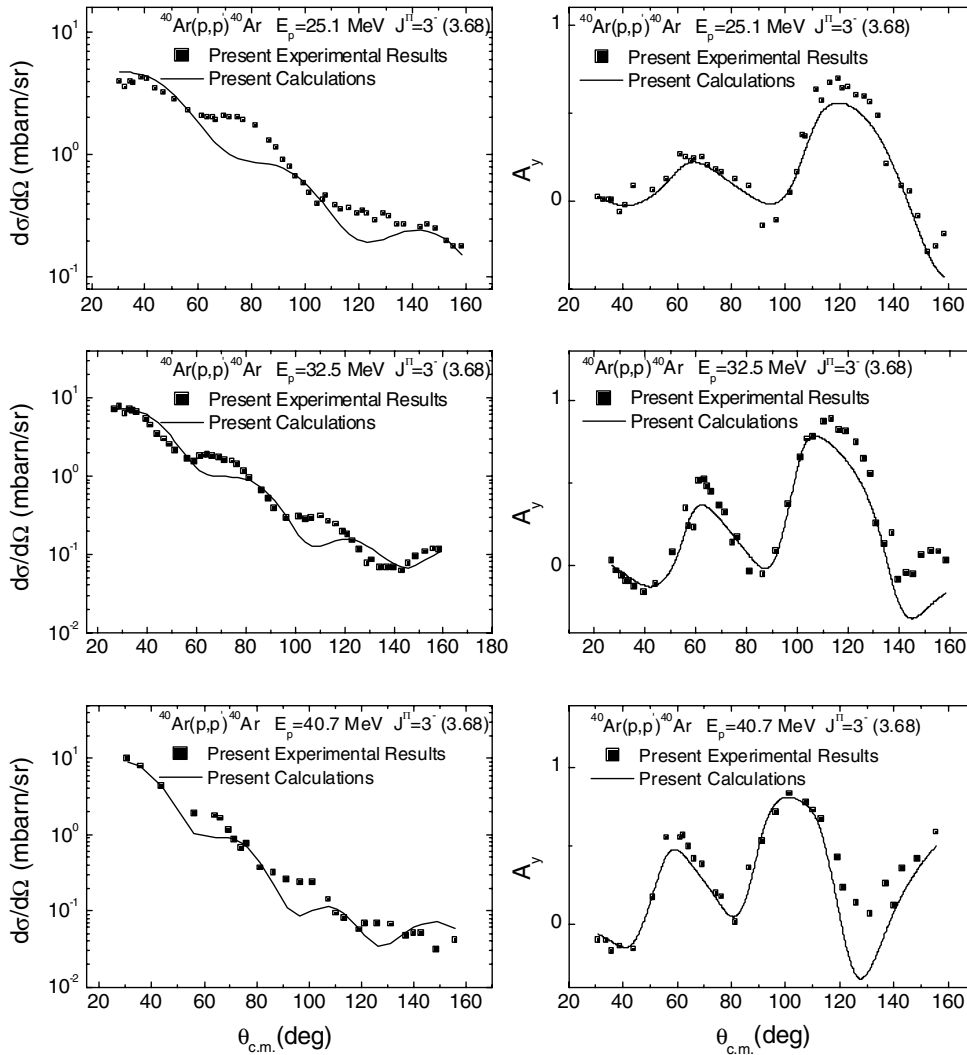
FIG. 4. Inelastic angular distributions (left) and analyzing powers (right) for proton scattering to the 3^- level of ^{40}Ar.

by taking account of the diffuseness of the charge density distribution of the form $f_c = [1 + \exp(r - R_c^0)/a_c]^{-1}$ [3].

In our formulation of the OMP in Eq. (5) the geometrical parameters of the Hartree-Fock (HF) potential r_{HF} and a_{HF} are in general different from the geometrical parameters r_v, a_v, r_s, a_s of the volume and surface absorptive potentials; however, the real and imaginary spin-orbit terms share the same r_{so} and a_{so} parameters. Therefore the volume dispersive contribution has different geometry (determined by r_v and a_v) from the real smooth volume potential (determined by r_{HF} and a_{HF}). As a result, we have two separate volume contributions to the potential (as can be seen in the first and second line of Eq. (5)), effectively giving us more flexibility than allowed by the optical model potential used in our previous work [10].

It is known that the energy dependence of the depth $V_{HF}(E)$ is due to the replacement of a microscopic nonlocal HF potential by a local equivalent. For a Gaussian nonlocality, $V_{HF}(E)$ is a linear function of E for large negative E and is an exponential for large positive E. Following Mahaux and Sartor [14], the energy dependence of the Hartree-Fock part of the nuclear mean field is taken as that found by

Lipperheide [15]:

$$V_{HF}(E) = A_{HF}\exp[-\lambda_{HF}(E - E_F)], \qquad (7)$$

where A_{HF} and λ_{HF} are undetermined constants with the latter associated with nuclear matter nonlocality range. Equation (7) can be used to describe the HF potential in the scattering regime [14]. The present optical potential includes relativistic corrections as discussed by Elton [16] and explained in our recent article [10].

It is useful to represent the variation of surface $W_s(E)$ and volume absorption potential $W_v(E)$ depth with energy in functional forms suitable for the dispersive optical model analysis. An energy dependence for the imaginary-surface term has been suggested by Delaroche *et al.* [17] to be:

$$W_s(E) = A_s \frac{(E - E_F)^2}{(E - E_F)^2 + (B_s)^2} \exp(-C_s|E - E_F|), \quad (8)$$

where A_s, B_s, and C_s are undetermined constants.

The isospin dependence of the potential (the Lane term [18,19]) was considered in real $V_{HF}(E)$ and imaginary surface
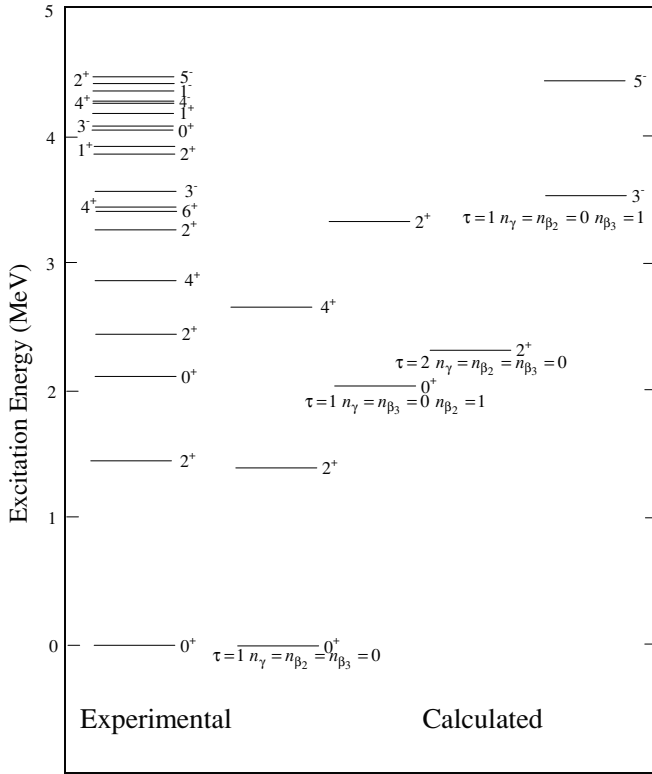
FIG. 5. Comparison of experimental low-lying collective levels of ^{40}Ar with those predicted by SRM.

$W_s(E)$ potentials as follows,

$$A_{HF} = V_0 \left[1 + (-1)^{Z'+1} \frac{C_{viso}}{V_0} \frac{N-Z}{A} \right] \quad (9)$$

$$A_s = W_0 \left[1 + (-1)^{Z'+1} \frac{C_{wiso}}{W_0} \frac{N-Z}{A} \right] \quad (10)$$

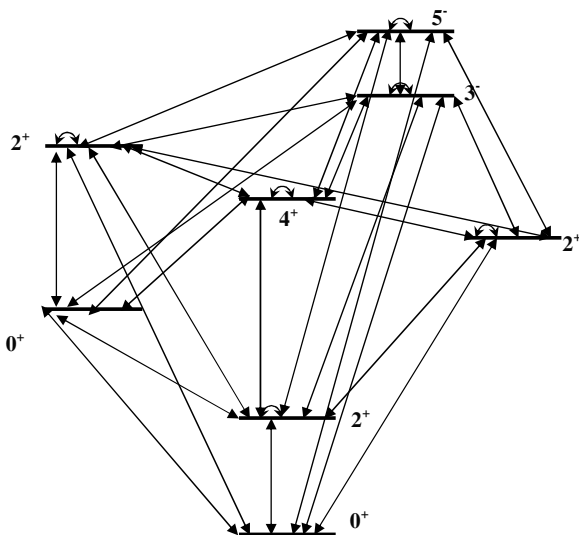where V_0, C_{viso}, W_0, and C_{wiso} are undetermined constants.

FIG. 6. Level coupling scheme used in the present calculations.

An energy dependence for the imaginary volume term has been suggested in studies of nuclear matter theory by Brown and Rho [20]:

$$W_v(E) = A_v \frac{(E - E_F)^2}{(E - E_F)^2 + (B_v)^2}, \quad (11)$$

where A_v and B_v are undetermined constants. The assumption that the imaginary potential $W_v(E)$ is symmetric about $E' = E_F$ is plausible for small values of $|E' - E_F|$; however, as was pointed out by Mahaux and Sartor [14], this approximate symmetry no longer holds for large values of $|E' - E_F|$. In fact the influence of the nonlocality of the imaginary part of the microscopic mean field will produce an increase of the empirical imaginary part $W(r, E')$ at large positive E' and approaches zero at large negative E' [21,22]. The DOM analysis of neutron scattering on ^{27}Al [23] and ^{232}Th [10] showed the importance of the dispersive contribution to describe σ_T data for energies above 100 MeV using a nonsymmetric version of the volume absorptive potential for large positive and large negative energies. Following Mahaux and Sartor [14], we assume that the absorption strengths are modified only outside some fixed energy interval around the Fermi energy $[E_F - E_a, E_F + E_a]$. They used $E_a = 60$ MeV; however, this value is fairly arbitrary [14] and we will use it as a fitting parameter. Let us assume that the nonlocal imaginary potential to be used in the dispersive integral is denoted by $\tilde{W}_v(E)$; then we can write [24]

$$\tilde{W}_v(E) = W_v(E) - W_v(E) \frac{(E_F - E - E_a)^2}{(E_F - E - E_a)^2 + E_a^2},$$

$$\text{for} \quad E < E_F - E_a \quad (12)$$

and

$$\tilde{W}_v(E) = W_v(E) + \alpha \left[\sqrt{E} + \frac{(E_F + E_a)^{3/2}}{2E} - \frac{3}{2}\sqrt{(E_F + E_a)} \right], \quad \text{for} \quad E > E_F + E_a. \quad (13)$$

These functional forms are chosen in such a way that the function and its first derivative are continuous at $E' = |E_F - E_a|$. At large positive energies nucleons sense the "hard core" repulsive region of the nucleon-nucleon interaction and $\tilde{W}_v(E)$ diverges like $\alpha \sqrt{E}$. Using a model of a dilute Fermi gas hard-sphere the coefficient α can be estimated to be equal to 1.65 MeV$^{1/2}$ [22], assuming that the Fermi impulse k_F is equal to 1.36 fm^{-1} and the radius of the repulsive hard core is equal to 0.4 fm. On the contrary, at large negative energies the volume absorption decreases and goes asymptotically to zero.

In a dispersion relation treatment, the real potential strength consists of a term which varies slowly with energy, the so-called Hartree-Fock term, $V_{HF}(\mathbf{r}, E)$, plus a correction term, $\Delta V(\mathbf{r}, E)$, which is calculated using a dispersion relation. Under favorable conditions of analyticity in the complex E plane the real part ΔV can be constructed from the knowledge of the imaginary part W on the real axis through the dispersion

relation

$$\Delta V(\mathbf{r}, E) = \frac{\mathcal{P}}{\pi} \int_{-\infty}^{\infty} \frac{W(\mathbf{r}, E')}{E' - E} dE', \qquad (14)$$

where we have now explicitly indicated the radial and energy dependence of these quantities and $\mathcal{P}$ means that the principal value of the integral should be taken. To simplify the problem, the geometry of the imaginary terms of the OMP are usually assumed to be energy independent and they are expressed in terms of a Woods-Saxon function $f_{\mathrm{ws}}[r, R_i(\theta', \varphi')]$ or its derivative $g_{\mathrm{ws}}[r, R_i(\theta', \varphi')]$. In such a case the radial functions factorize out of the integrals and the energy dependence is completely accounted for by two overall multiplicative strengths, $\Delta V(E)$ and $W(E)$. Both of these factors contain, we note, volume and surface contributions. The dispersive treatment employed in this work to calculate dispersive contributions $\Delta V_v(E)$, $\Delta V_s(E)$, and $\Delta V_{so}(E)$ was described in detail in Ref. [10], so we refer interested readers to that contribution.

IV. ANALYSIS OF EXPERIMENTAL DATA

Experimentally determined inelastic-scattering data for 2^+(1.46 MeV) and 3^-(3.68 MeV) level excitations for the three incident proton energies along with the elastic-scattering data for these energies [5] were analyzed simultaneously with the neutron total cross sections to get a unique ^{40}Ar-nucleon (neutron-proton differences in the optical potential are described by its isospin dependence, Eq. (9)) optical potential in the 1- to 100- MeV energy region. The optical potential parameters were searched to reproduce the neutron and proton cross-section data by minimizing the quantity χ^2 defined by

$$\chi^2 = \frac{1}{N+M} \left[\sum_{i=1}^{N} \frac{1}{K_i} \sum_{j=1}^{K_i} \left(\frac{d\sigma_{ij}/d\Omega_{\mathrm{calc}} - d\sigma_{ij}/d\Omega_{\mathrm{exp}}}{\Delta d\sigma_{ij}/d\Omega_{\mathrm{exp}}} \right)^2 \right.$$
$$\left. + \sum_{i=1}^{M} \left(\frac{\sigma_{\mathrm{tot}_{\mathrm{cal}_i}} - \sigma_{\mathrm{tot}_{\mathrm{eval}_i}}}{\Delta \sigma_{\mathrm{tot}_{\mathrm{eval}_i}}} \right)^2 \right] \qquad (15)$$

where $d\sigma_{ij}/d\Omega_{\mathrm{exp}}$ and $d\sigma_{ij}/d\Omega_{\mathrm{calc}}$ are experimental and calculated angular distribution data, whereas $\sigma_{\mathrm{tot}_{\mathrm{eval}_i}}$ and $\sigma_{\mathrm{tot}_{\mathrm{cal}_i}}$ are measured and evaluated total cross sections all with their assigned errors. N denotes the number of experimental scattering data sets, K_i the number of angular points in each scattering data set, and M the number of energies for which experimental (evaluated) neutron total cross section data are involved.

The optical model code OPTMAN [9,25] was used for OMP parameter fitting. We used symmetric surface and non-symmetric volume imaginary absorptive potentials, therefore we initially adjusted 16 parameters, namely $V_0, \lambda_{\mathrm{HF}}, C_{\mathrm{viso}}$, which define the smooth energy dependence of the real volume potential; $W_0, C_{\mathrm{wiso}}, B_s, C_s$ and A_v, B_v, E_a defining the surface and volume absorptive potential, respectively, plus six geometrical parameters ($r_{\mathrm{HF}}, a_{\mathrm{HF}}, r_v, a_v, r_s, a_s$). After proper values were obtained by this global minimization, spin-orbit parameters $V_{\mathrm{so}}, \lambda_{\mathrm{so}}, A_{\mathrm{so}}, B_{\mathrm{so}}, r_{\mathrm{so}}$ and a_{so}, parameters of the Coulomb interaction, C_{Coul}, r_c, and a_c and equilibrium deformation parameters $\beta_{\lambda 0}$ ($\lambda = 2, 3, 4$ for quadrupole, octupole, and hexadecapole deformations accordingly) were also optimized. The final iteration involved a free variation of all parameters using the best-fit search option of the OPTMAN code. The derived dispersive CCOMP (DCCOMP) potential parameters are listed in Table II. The attained minimum χ^2 value, as defined by Eq. (15), was 2.7.

V. RESULTS AND DISCUSSION

As shown in Table I, the softness of the ^{40}Ar nucleus to quadrupole deformations, $\mu_{\beta_{20}}$, is found to be rather large, namely 2.0585. Typical rotational nuclei such as actinides have $\mu_{\beta_{20}}$ values of 0.1 to 0.3 [26], and ^{56}Fe has a value of about 0.5 [27]. The larger $\mu_{\beta_{20}}$ signifies that a nucleus is soft to quadrupole deformation. This leads to a significant enhancement of coupling strength between the levels. For instance, the "effective" quadrupole deformation determining one step excitation of the first 2^+ level is enhanced by a factor of 2.75 compared with the rigid case having the same equilibrium-quadrupole deformation β_{20}. In the present example, the ground-state quadrupole deformation was found

TABLE II. Dispersive coupled-channel OMP parameters for ^{40}Ar. We used the following deformation parameters: $\beta_{20} = 0.0805$, $\beta_4 = 0.312$, $\beta_{30} = \beta_{20}\varepsilon = 0.11135$ for ^{40}Ar.

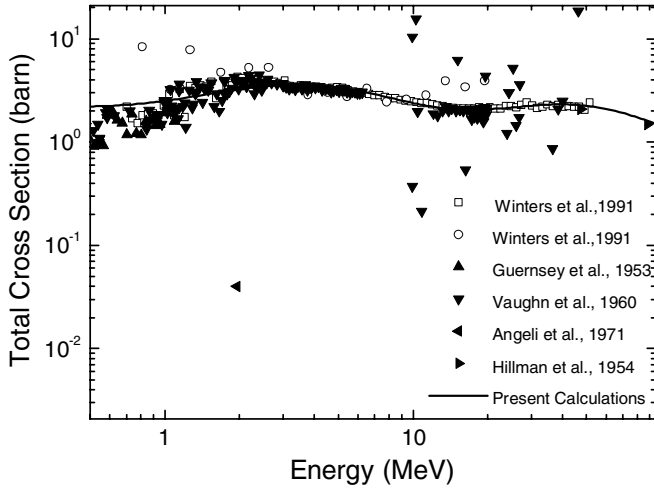|	Volume	Surface	Spin-orbit	Coulomb
Real depth (MeV)	$V_0 = 53.24$ $\lambda_{\mathrm{HF}} = 0.00978$ $C_{\mathrm{viso}} = 8.0$	dispersive	$V_{\mathrm{so}} = 6.33$ $\lambda_{\mathrm{so}} = 0.005$	$C_{\mathrm{Coul}} = 2.00$
Imaginary depth (MeV)	$A_v = 9.15$ $B_v = 81.82$ $E_a = 132.0$	$W_0 = 10.75$ $B_s = 12.56$ $C_s = 0.01035$ $C_{\mathrm{wiso}} = 21.0$	$W_{\mathrm{so}} = -3.1$ $B_{\mathrm{so}} = 160$	
Geometry (fm)	$r_{\mathrm{HF}} = 1.2223$ $a_{\mathrm{HF}} = 0.637$ $r_v = 1.0971$ $a_v = 0.734$	$r_s = 1.1686$ $a_s = 0.528$	$r_{\mathrm{so}} = 1.1293$ $a_{\mathrm{so}} = 0.586$	$r_c = 1.0614$ $a_c = 0.638$

FIG. 7. Comparison of predicted and experimental ^{40}Ar neutron total cross sections. Experimental data from EXFOR are shown by various symbols.

to be 0.0805, but the effective value is enhanced to a value of 0.22. This value is in close agreement with the β_2 determined from $B(E2)$ [28]. Similarly, enhancement of the coupling between the ground state and the 3^- state is 2.778, giving the effective β_3 to be $0.11135 \times 2.778 = 0.309$. This is favorably compared with the value of 0.31 deduced from $B(E3)$ data [29]. Therefore, the SRM effectively gives a reasonable picture that ^{40}Ar has a small static but a large dynamic deformation, which means that this nucleus is more like a vibrational than a rotational one. It will be worth noting that such enhancements are radically different for different pairs of levels.

Optical model calculations with the best fit parameters listed in Table II nicely describe available experimental ^{40}Ar neutron total data from about 1- to 100- MeV incident energies, as seen in Fig. 7.
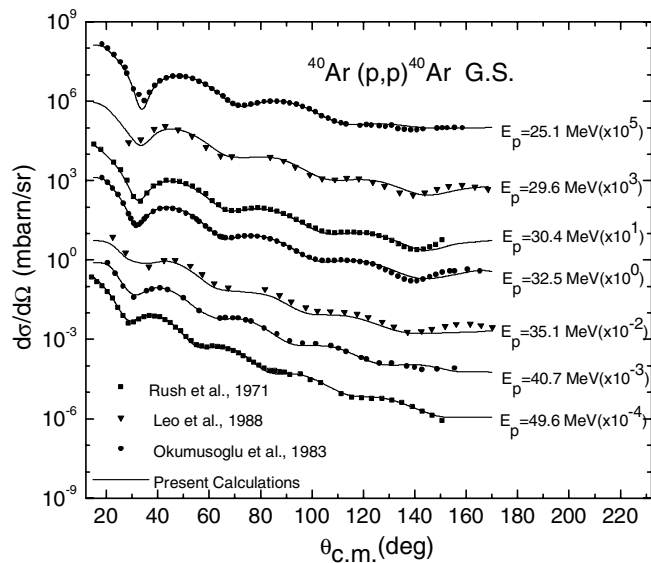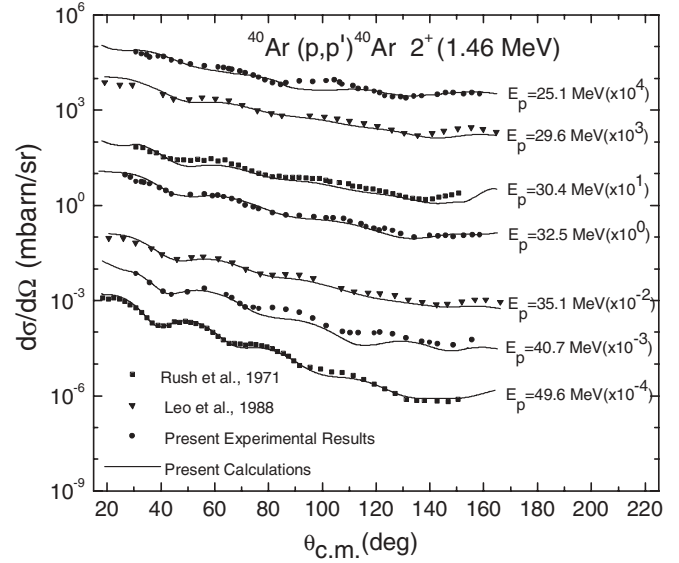

FIG. 9. Available 2^+ experimental inelastic angular distributions compared with DCCOMP predictions.

Comparison of our experimentally measured ^{40}Ar angular distributions with those predicted by the DCCOM calculations using the best fit potential is shown in Figs. 2–4. One can see that DCCOMP describes scattering data measured, yet the description of the fine angular structure is not as good, perhaps due to uncertainties in separating elastic and inelastic peaks. Theoretical predictions of analyzing powers, shown on the right sides of Figs. 2–4, show much better agreement with experiment. As the OPTMAN code has no option to calculate analyzing powers, the ECIS code [30], with three levels coupled, using our best fit optical parameters, was used for such calculations. In Figs. 8–10 our experimental data are shown along with other proton angular distributions available in this energy region. One can that see our experimental data
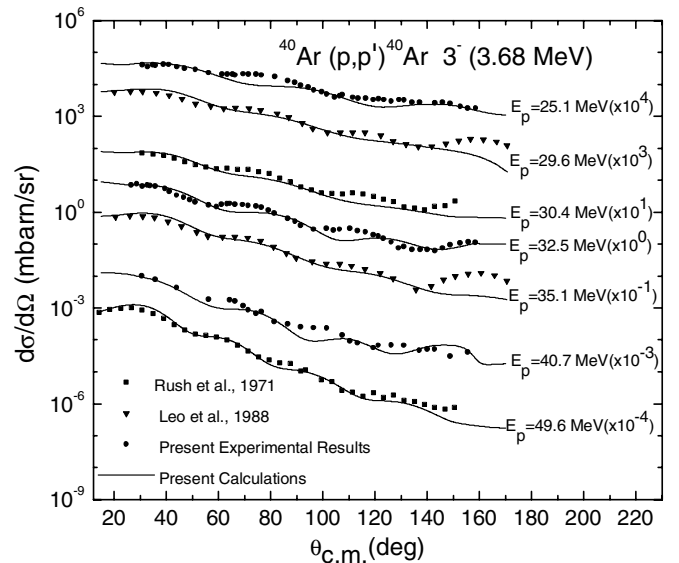

FIG. 8. Available experimental elastic angular distributions compared with DCCOMP predictions.

FIG. 10. Available 3^- experimental inelastic angular distributions compared with DCCOMP predictions.

are consistent with the other proton-scattering data, so that the best fit potential determined with DCCOMP can describe all of the data simultaneously.

The derived optical potential energy dependence is very simple. We do not need to introduce energy-dependent geometry and the potential parameters are commonly applicable for both neutron and proton projectiles. The dispersion relations, coupled to the smooth energy-dependent Hartree-Fock potential $V_{HF}(E)$, fully determine the real part of the dispersive contribution once the imaginary part of the mean field is fixed. Very few parameters are required in comparison with a conventional nondispersive coupled-channel OMP analysis.

VI. CONCLUSIONS

We have applied the SRM-CC (a coupled-channels method based on the coupling built on soft-rotator model wave functions) to analyze the low-lying collective level structure and nucleon interaction with ^{40}Ar. The description of the collective levels by the present model turned out to be in a reasonable success, giving that this nucleus is soft to quadrupole and octupole deformations. This picture is consistent with the fact that it has a small ground-state quadrupole moment, but the collective levels are excited quite strongly; namely it is a vibrational-like nucleus. In fact, our approach yielded a small equilibrium deformations but large dynamical deformations due to softness of both the quadrupole and octupole deformations.

In this work we have presented new experimental data for protons with incident energies of 25.1, 32.5, and 40.7 MeV scattered by ^{40}Ar nuclei elastically and inelastically, exciting the 2^+(1.46-MeV) and 3^-(3.68-MeV) levels. The use of these high-energy proton-scattering data along with neutron total cross-section data simultaneously in a dispersive isospin-dependent "relativistic" coupled-channels optical model analysis of nucleon scattering on ^{40}Ar nuclei from 1 to 100 MeV made it possible to increase the accuracy of estimated optical potential parameters, especially in the high-energy region. Good overall agreement obtained between predictions and experimental data became possible due to including dispersive terms and accounting for nonlocality effects in the optical model potential and CC calculations.

The isovector terms give the possibility to extend the derived potential parameters to neighboring nuclei with great confidence. The resulting data have been forwarded to the international experimental data base EXFOR (EXFOR #C1329004. For the elastic scattering data submitted previously see EXFOR #C1329003).

[1] E. Sh. Sukhovitskiĭ, Y. O. Lee, J. Chang, S. Chiba, and O. Iwamoto, Phys. Rev. C **62**, 044605 (2000).

[2] E. S. Sukhovitskiĭ, S. Chiba, J.-Y. Lee, B.-t. Kim, and S.-W. Hong, J. Nucl. Sci. Technol. **40**, 69 (2003).

[3] S. Chiba, O. Iwamoto, Y. Yamanouti, M. Sugimoto, M. Mizumoto, K. Hasegawa, E. S. Sukhovitskiĭ, Y. V. Porodzinskiĭ, and Y. Watanabe, Nucl. Phys. **A624**, 305 (1997).

[4] W. Sun, Y. Watanabe, E. S. Sukhovitskiĭ, O. Iwamoto, and S. Chiba, J. Nucl. Sci. Technol. **40**, 635 (2003).

[5] N. T. Okumusoglu, J. Birchall, M. S. A. L. Al Ghazi, C. Lapointe, J. S. C. McKee, H. E. Conzett, R. M. Larimer, and P. von Rossen, Nucl. Phys. **A393**, 45 (1983).

[6] A. A. Rush, E. J. Burge, and D. A. Smith, Nucl. Phys. **A166**, 378 (1971).

[7] E. A. Silverstein, Nucl. Instrum. Methods **4**, 53 (1959).

[8] A. D. Bacher, G. R. Plattner, H. E. Conzett, D. J. Clark, H. Grunder, and W. F. Tivol, Phys. Rev. C **5**, 1147 (1972).

[9] E. Sh. Soukhovitskiĭ, S. Chiba, O. Iwamoto, K. Shibata, T. Fukahori, and G. B. Morogovskiĭ, *Programs OPTMAN and SHEMMAN Version 8*. Technical report, JAERI-Data/Code 2005-002, Japan Atomic Energy Research Institute, 2005.

[10] E. Sh. Soukhovitskiĭ, R. Capote, J. M. Quesada, and S. Chiba, Phys. Rev. C **72**, 024604 (2005).

[11] E. Sh. Soukhovitskiĭ, R. Capote, J. M. Quesada, and S. Chiba, Varenna Conference June 2006 (to be published).

[12] E. Sh. Sukhovitskii, Y. O. Lee, J. W. Chang, S. Chiba, and O. Iwamoto, Phys. Rev. C **62**, 044605 (2000).

[13] R. H. Bassel, R. M. Drisko, and G. R. Satchler, Technical report ORNL-3240, Oak Ridge National Laboratory, 1962.

[14] C. Mahaux and R. Sartor, Nucl. Phys. **A528**, 253 (1991).

[15] R. Lipperheide, Z. Phys. **202**, 58 (1967).

[16] R. B. L. Elton, Nuovo Cimento B **43**, 227 (1966).

[17] J. P. Delaroche, Y. Wang, and J. Rapaport, Phys. Rev. C **39**, 391 (1989).

[18] A. M. Lane, Phys. Rev. Lett. **8**, 171 (1962).

[19] A. M. Lane, Nucl. Phys. **35**, 676 (1962).

[20] G. E. Brown and M. Rho, Nucl. Phys. **A372**, 397 (1981).

[21] C. Mahaux and H. Ngô, Nucl. Phys. **A431**, 486 (1984).

[22] C. Mahaux and R. Sartor, Nucl. Phys. **A458**, 25 (1986).

[23] A. Molina, R. Capote, J. M. Quesada, and M. Lozano, Phys. Rev. C **65**, 034616 (2002).

[24] C. Mahaux and R. Sarto, *Advances in Nuclear Physics*, edited by J. W. Negele and E. Vogt (Plenum, New York, 1991), Vol. 20.

[25] E. S. Soukhovitskiĭ, G. B. Morogovskiĭ, S. Chiba, O. Iwamoto, and T. Fukahori, *Physics and Numerical Methods of OPTMAN: A Coupled-channels Method Based on Soft-rotator Model for a Description of Collective Nuclear Structure and Excitation*, Technical report, JAERI-Data/Code 2004-002, Japan Atomic Energy Research Institute, 2004.

[26] O. Iwamoto, S. Chiba, and R. Kuwata, J. Nucl. Sci. Technol. **34**, 490 (1997).

[27] E. S. Soukhovitskiĭ, S. Chiba, J.-Y. Lee, Y.-O. Lee, J. Chang, T. Maruyama, and O. Iwamoto, J. Nucl. Sci. Technol. **39**, 816 (2002).

[28] S. Raman, C. W. Nestor, Jr., and P. Tikkanen, At. Data Nucl. Data Tables **78**, 1 (2001).

[29] T. Kibedi and R. H. Spear, At. Data Nucl. Data Tables **80**, 35 (2002).

[30] J. Raynal, Notes on ECIS, CEA-N-2772, (1994).